LA-UR-79-1582

MASTER

Conf-790381--2

TITLE: PREDICTED VERSUS OBSERVED COSMIC-RAY-PRODUCED NOBLE GASES IN LUNAR SAMPLES: IMPROVED KR PRODUCTION RATIO

AUTHOR(S): S(erge) Regnier, Univ. Calif., San Diego

C(harles) M. Hohenberg, Washington Univ., St. Louis MO

K(urt) Marti, Univ. Calif., San Diego

R(obert) C. Reedy, Los Alamos Sci. Lab

SUBMITTED TO: Proceedings of the Tenth Lunar and Planetary Science Conference.

los alamos scientific laboratory
of the University of California
LOS ALAMOS, NEW MEXICO 87545

An Affirmative Action/Equal Opportunity Employer

Form No. 836
St. No. 2629
1/75

UNITED STATES
ENERGY RESEARCH AND
DEVELOPMENT ADMINISTRATION
CONTRACT W-7405-ENG. 36

Predicted versus Observed Cosmic-Ray-Produced Noble Gases in Lunar Samples: Improved Kr Production Ratios

S. Regnier[1,2], C. M. Hohenberg[3], K. Marti[1], and R. C. Reedy[4]

Submitted to the Proceedings of the Tenth Lunar and Planetary Science Conference.

April 27, 1979

Revised June 7, 1979

1. Department of Chemistry, University of California, San Diego CA 92093.
2. Present address: Centre d'Études Nucléaires de Bordeaux-Gradignan, Le Haut-Vigneau, 33170 Gradignan, France.
3. Department of Physics and McDonnell Center for the Space Sciences, Washington University, St. Louis MO 63130.
4. Los Alamos Scientific Laboratory of the University of California, Los Alamos NM 87545.

ABSTRACT

New sets of cross sections for the production of krypton isotopes from targets of Rb, Sr, Y, and Zr have been constructed primarily on the bases of experimental excitation functions for Kr production from Y. These cross sections were used to calculate galactic-cosmic-ray and solar-proton production rates for Kr isotopes in the moon. We report spallation Kr data obtained from ilmenite separates of rocks 10017 and 10047. Production rates and isotopic ratios for cosmogenic Kr observed in ten well-documented lunar samples and in ilmenite separates and bulk samples from several lunar rocks with long but unknown irradiation histories were compared with predicted rates and ratios. The agreements were generally quite good. Erosion of rock surfaces only affected rates or ratios for near-surface samples where solar-proton production is important. There were considerable spreads in predicted-to-observed production rates of ^{83}Kr, due at least in part to uncertainties in chemical abundances. The ^{78}Kr/^{83}Kr ratios were predicted quite well for samples with a wide range of Zr/Sr abundance ratios. The calculated ^{80}Kr/^{83}Kr ratios were greater than the observed ratios when production by the ^{79}Br(n,γ) reaction was included, but were slightly undercalculated if the Br reaction was omitted, suggesting that Br(n,γ)-produced Kr is not retained well by lunar rocks. The productions of ^{81}Kr and ^{82}Kr were overcalculated by approximately 10% relative to ^{83}Kr. Predicted-to-observed ^{84}Kr/^{83}Kr ratios scattered considerably, possibly due to uncertainties in corrections for trapped and fission components and in cross sections for ^{84}Kr production. Most predicted ^{84}Kr and ^{86}Kr production rates are lower than observed. Shielding depths of several Apollo 11 rocks were determined from the measured ^{78}Kr/^{83}Kr ratios of ilmenite separates.

approach which calculates the production rates of spallogenic nuclei on the bases of nuclear-reaction cross sections and cosmic-ray flux models (e.g., Reedy and Arnold, 1972). In Hohenberg et al. (1978), a comprehensive comparison was made between these two approaches by comparing observed and calculated cosmogenic neon, argon, krypton, and xenon production rates and isotopic ratios in well-documented lunar samples with simple exposure histories. While good agreement was found for most noble gases, significant discrepancies were observed for the production rates and ratios for the Kr isotopes. The calculated ^{84}Kr/^{83}Kr ratios were considerably greater than the observed ratios, and the calculated variations of the ^{78}Kr/^{83}Kr ratio with different Zr/Sr ratios were opposite the observed trend.

Hohenberg et al. (1978) attributed much of these Kr disagreements to the lack of experimental excitation functions with which to calculate theoretical production rates; the only measured cross sections available to them were for Kr production from strontium by protons at 0.73 GeV (Funk et al., 1967). Cross sections are now available for all Kr isotopes produced in yttrium targets by protons at 0.08, 0.15, 1.05 and 24 GeV (Regnier, 1979). These Y(p,x)Kr excitation functions have been used to help establish Kr-production systematics with which to estimate cross sections for targets and energies for which there are no experimental data.

This paper describes these new Kr production cross sections and uses them to calculate production rates of $^{78-86}$Kr from targets of Rb, Sr, Y, and Zr as a function of depth in the moon. The calculated production rates and isotopic ratios are compared with the cosmogenic Kr observed in lunar samples, including all the samples used by Hohenberg et al. (1978). Cosmogenic Kr isotopic ratios for bulk samples and ilmenite separates from three Apollo 11 rocks are used to check the predicted systematics of Kr production from Zr and to infer the effective depth at which these rocks received their exposure.

THEORETICAL SYSTEMATICS

The theoretical production rates of spallogenic Kr isotopes were calculated using the models of Reedy and Arnold (1972). The production rate for a given product nucleus from an elemental target at one shielding depth was calculated by integrating over energy the product of the cosmic-ray particle flux at that depth and the cross section for the production of the product from that target. The cosmic-ray particle fluxes were the same as those used by Hohenberg et al. (1978). For solar cosmic rays (SCR), only solar protons with an omnidirectional flux of 70 protons/cm^2 s above 10 MeV and an exponential-rigidity spectrum with R_o = 100 MV were considered. The fluxes of galactic-cosmic-ray (GCR) particles above 1 MeV as a function of depth were the semi-infinite plane ones of Reedy and Arnold (1972).

The excitation functions used for the production of Kr by spallation reactions of protons with targets of Rb, Sr, Y, and Zr are discussed below. For reactions induced by the secondary neutrons produced by the galactic cosmic rays, the proton-induced cross sections were assumed. This assumption should not seriously affect calculated GCR production rates because most reactions considered here require large energies to produce a given nuclide from a specific target and such cross sections are usually insensitive to the incident particle. Probably the most important neutron-induced reaction omitted here is ^{86}Sr(n,α)^{83}Kr, for which there are no measured cross sections and which could have cross sections significantly different from those for the ^{86}Sr(p,α)^{83}Rb reaction. To see the relative importance of the ^{86}Sr(n,α)^{83}Kr reaction in producing ^{83}Kr from strontium, an excitation function was made for this reaction assuming a peak cross section of 10 millibarns at a neutron energy of 16 MeV (similar to measured values for nearby nuclei). The production rates calculated for ^{83}Kr by this (n,α) reaction were about 1% of those calculated for the Sr(p,x)^{83}Kr reaction. Thus there is no indication that the use of only proton-induced cross sections will affect calculated GCR production rates.

Slow neutrons with energies below ~0.5 MeV can produce ^{80}Kr and ^{82}Kr via neutron-capture reactions with bromine. As in Hohenberg et al. (1978), the reaction rates used for the $^{79}Br(n,\gamma)$ and $^{81}Br(n,\gamma)$ reactions as a function of depth were the theoretical ones of Lingenfelter et al. (1972) multiplied by the neutron-density normalization factor of 0.8 determined by the Apollo 17 Lunar Neutron Probe Experiment (Woolum et al., 1975).

Excitation Functions

In lunar samples, spallation Kr is produced predominantly by high-energy reactions in Sr, Y, and Zr, but low-energy particle reactions on Rb are responsible for significant contributions to the heaviest Kr isotopes. Some Kr isotopes receive contributions from both β^- and β^+ or ε decay chains. In particular, ^{83}Kr represents the total isobaric yield for mass 83. $^{84,86}Kr$ are shielded by stable isotopes of Sr on the neutron-deficient side of the isobar. For spallogenic Kr, the only available experimental results are the measurement of $^{78-85}Kr$ produced in Sr bombarded by 730 MeV protons (Funk et al., 1967), and the measurement of $^{78-86}Kr$ produced in Y bombarded by 80, 150, 1050, and 24000 MeV protons (Regnier, 1979). The excitation functions of spallation reactions for other energies and targets were estimated by using semi-empirical considerations.

A compilation was prepared of all available cross sections for reactions of similar target-to-product mass loss (ΔA) in the same mass range of targets. The most useful information was obtained from the works by Morrison and Caretto (1962) (p,xp reactions), Remsberg and Miller (1963) (p,pxn reactions), Korteling and Hyde (1964) (^{93}Nb + p), Caretto and Wiig (1956) (^{89}Y + p), Strohal and Caretto (1961) (^{96}Zr + p), Unseren and Wiig (1961) (^{90}Zr + p), Caretto and Wiig (1959) (^{89}Y + p), Porile et al. (1963) (^{69}Ga and ^{71}Ga + p), Rudstam and Bruninx (1961) (^{75}As + p), and Sachdev et al. (1967) (^{88}Sr + p). Excitation functions were then estimated by summation over all possible reaction channels using nuclear systematics from similar (p,xpyn) reactions. Analogy with the production of Kr in ^{89}Y was used as often as possible. Other factors in the systematics are the ΔA between target and product and the N/Z ratio of the target. In the case of low-energy incident particles, all possible reaction channels were taken into account. This approach gives more complete results than semi-empirical formulae, from which good estimates can be obtained only for high-energy particles.

The excitation functions used for the production of $^{78-86}Kr$ from targets of Rb, Sr, Y, and Zr are shown in Figs. 1 and 2. The production cross-sections were estimated from the threshold energy to several GeV. ^{78}Kr (Fig. 1) is a high-energy product in all four targets, the lowest ΔA occurring in the $^{85}Rb(p,2p6n)^{78}Kr$ reaction. Due to a lack of information, the excitation function of ^{78}Kr from Rb is rather uncertain. Analogy with Y was the most important factor in estimates for other targets. ^{80}Kr (Fig. 1) is also a high-energy product in Sr, Y, and Zr, and analogy considerations to Y were also predominant. In the case of Rb, (p,α2n) and (p,3p3n) reactions are responsible for the two peaks at low energy. ^{81}Kr (Fig. 1) is produced by (p,αn) and (p,p4n) reactions in ^{85}Rb. High-energy reactions are also predominant for other targets except for the important channel (p,2αn) in ^{89}Y.

The case of ^{82}Kr becomes more complicated because ΔA is smaller and low-energy production becomes significant. Also, the number of important reaction channels is increasing. The excitation functions (Fig. 1) are the sum of all possible channels for low-energy particles, in particular (p,αn) and (p,pα) for Sr and (p,2α) for Y. ^{83}Kr (Fig. 2) in Rb results from (p,3n), (p,p2n), and (p,2pn) reactions, yielding high cross sections at low energy. Important channels in Sr are (p,α) and (p,3p3n) reactions. Analogy to Y was used in the case of Zr.

^{84}Kr (Fig. 2) in Rb is made by several highly probable channels in both ^{85}Rb and ^{87}Rb, in particular ^{85}Rb(p,pn) and ^{87}Rb(p,p3n) and (p,α) reactions. Low-energy reactions are also important in the cases of ^{88}Sr(p,αn) or ^{89}Y(p,3p3n). ^{84}Kr in Zr is only a high-energy product. ^{86}Kr (Fig. 2) is produced by single-channel, low-cross-section reactions: ^{87}Rb(p,2p), ^{88}Sr(p,3p), and ^{89}Y(p,4p). The excitation function in Zr is only tentative, especially for the heaviest isotopes of this target, so there are considerable uncertainties in the cross sections. It will be noted by looking at Fig. 2 that, at least in the case of meteorites, Rb could be a rather important target element for the production of $^{84-86}$Kr.

Some experimental data would clearly be useful. For Zr as a target, only particles of E > 100 MeV can produce spallation Kr in significant amounts. For targets of Rb and Sr, several measurements at energies below 100 MeV are needed in addition to high-energy cross sections.

Calculated Cosmogenic Production Rates

The calculated production rates for Kr isotopes from Rb, Sr, Y, and Zr at various shielding depths in the moon are presented in Table 1 in units of atoms per minute per kilogram of target element (1 atom/min/kg = 1.96 x 10^{-11} cm^{3}STP/g/m.y.) The general trends for variations of production rates with depth are similar to those reported by Hohenberg _et al._ (1978), e.g., ^{78}Kr showing little increase in production rate with increasing depth near the surface and ^{83}Kr having its maximum GCR production rate at a depth of about 30 g/cm^2. The change in the ^{78}Kr/^{83}Kr ratio with increasing depth is less for the heavier targets, consistent with the larger threshold energies for reactions with these targets (see Fig. 3). Major changes relative to previously calculated Kr production rates involve those for ^{78}Kr and ^{84}Kr relative to ^{83}Kr. The ^{78}Kr/^{83}Kr ratios in Zr and Y are now predicted to be systematically larger than those in Sr, consistent with a trend previously observed empirically (Marti _et al._, 1973). The production rates for ^{84}Kr from Sr and Y are considerably smaller than previously calculated.

For comparisons with empirical cosmogenic Kr rates and ratios inferred from observed data, "predicted" qualities were determined from these calculated production rates. The elemental abundances of the five important target elements - Rb, Sr, Y, Zr, and Br - were compiled for each lunar sample. At a given depth, the production rate of a particular Kr isotope can be obtained by summing the products of elemental abundances and elemental production rates. These predicted rates are only applicable if the lunar rock did not experience any erosion of its surface while on top of the regolith. For 2.1 x 10^5-y ^{81}Kr, the depth of the sample in the recovered rock was always used in predicting its production rate. For the stable Kr isotopes in most rocks, surface erosion must be considered.

Estimates of the rate of surface erosion on the moon have been made by a variety of techniques. The density-versus-depth profile of energetic particle tracks indicates that an average erosion rate of 0.3 g/cm^2 per million years applies to several different lunar samples (Crozaz et al., 1972; Yuhas, 1974); the depth distribution of cosmic-ray-produced radionuclides suggests a distribution of erosion rates ranging from 0.15 to 0.6 g/cm^2 per million years for various other lunar samples (Wahlen et al., 1972). In reality the surface erosion rate for a particular lunar sample is likely to be reasonably dependent upon geometry and the mechanical properties of the sample.

In this paper, we assume an average erosion rate of 0.3 g/cm^2 per million years. Surface erosion is explicitly considered in the predictive systematics presented here. For instance, sample 14306,26 has an exposure age of 25.4 million years and was recovered from a depth of 7 g/cm^2. An erosion rate of 0.3 g/cm^2 per million years would imply a total of 7.6 g/cm^2 would have been removed. The resulting production rates for all Kr isotopes except ^{81}Kr are computed by integrating the effects of exposure starting at an initial depth of 14.6 g/cm^2 to a final depth of 7 g/cm^2. Comparisons with spectra computed with the assumption of no erosion indicate the relative importance of erosion for various samples. In general, erosion is relatively more important for samples which are very close to the surface and for the heavier Kr isotopes, which are made in significant quantities by SCR particles.

EMPIRICAL SYSTEMATICS FROM OBSERVED KR

Several classes of lunar samples were selected to provide an empirical or observational data base for comparisons with predicted systematics for cosmogenic Kr. For comparisons of both absolute production rates and isotopic ratios, well-documented samples with simple exposure histories were used. The criteria for selecting such samples (Hohenberg et al., 1978) include: 1) using pieces of small rocks; 2) having target-element and noble-gas data; 3) knowing absolute exposure ages from ^{81}Kr-^{83}Kr determinations; 4) having exposure ages which are less than about 50 million years so erosion effects and other shielding changes such as turnover are minimal; and 5) knowing the depths for shielding from the cosmic rays. The same ten samples selected by Hohenberg et al.(1978) for Kr comparisons were used here.

For all samples, the observed Kr was corrected for fission and trapped components. Krypton produced by the spontaneous fission of ^{238}U was removed assuming an accumulation time of 3.9 x 10^9 years; this correction is very small for the samples considered here. The remaining Kr is assumed to be a superposition of cosmogenic Kr and trapped Kr with the BEOC-12 composition determined by Eberhardt et al. (1972). Cosmogenic ^{86}Kr is estimated from the (fission-corrected) ^{86}Kr/^{83}Kr ratio assuming cosmogenic ^{86}Kr/^{83}Kr = 0.015 ± 0.015

(Marti and Lugmair, 1971). Cosmogenic contributions to other Kr isotopes are obtained by subtraction of a BEOC-12 composition based on the trapped ^{86}Kr. For most samples, these corrections are relatively minor. However, in certain samples, especially those with short exposure ages, the cosmogenic component for some isotopes, e.g., ^{84}Kr, can have a fairly large uncertainty.

To expand the observational data base, Hohenberg et al. (1978) selected another set of samples in which the cosmogenic component was enhanced relative to other components. Because such samples generally have had substantially longer exposures than the well-documented samples, it is almost certain that they have experienced significant shielding changes during their exposure histories, and no generally applicable and testable techniques are available for deciphering such histories. Also, because the ^{81}Kr-^{83}Kr exposure age calculation necessarily assumes exposure at a single shielding depth, we cannot make determinations of total exposure time, and thus absolute production rates are not determinable.

The spallation ratio ^{78}Kr/^{83}Kr was recognized to be a very useful parameter for the evaluation of shielding conditions during cosmic-ray irradiation (Marti and Lugmair, 1971). However, this same ratio was observed to be affected also by differences in the relative abundances of the major target elements Sr and Zr (e.g., Marti et al., 1973; Eberhardt et al., 1974). Eberhardt and coworkers (1974) have studied the dependence on target element composition in lunar rock 10071 by concentrating Zr and Sr in mineral separates of ilmenite and feldspar, respectively. They have demonstrated that the relative ^{78}Kr yield is enhanced in Zr as the target and depressed in Sr. We have extended this approach to two additional Apollo 11 rocks in order to evaluate spallation systematics and to decouple the target element dependence from the shielding or hardness parameter. Ilmenite separates were obtained from rocks 10017 and 10047 by a combination of heavy liquid separations, crushing the sinks to <88 μm and by handpicking of impurities. The data are compiled in Table 2, including data of Eberhardt et al. (1974) for completeness. Spallation components were calculated by subtracting trapped Kr from the measured data and by adjusting $(^{86}Kr/^{83}Kr)_{spall}$ to 0.015. This Kr ratio is a measured quantity (Marti and Lungmair, 1971) and may still include a small trapped component of unknown magnitude. Also, as pointed out earlier, the relative ^{86}Kr yield from Zr might possibly be somewhat larger, due to a contribution from the heavy Zr isotopes. The exposure history and shielding conditions of the above three Apollo 11 basalts are not well-known, although precise ^{81}Kr-Kr ages have been determined. However, we can calculate an average effective shielding condition for the ilmenite separates (for which Zr is expected to be the only target) and then calculate the expected spallation Kr components for the bulk-rock samples and compare the results to the measured mass yield. This should provide a crucial test of the applicability of our calculations to samples of varying target element composition.

DISCUSSION

In Table 3 we compare the predictions for Kr production rates and isotopic ratios with observations for the ten well-documented samples. The average (and standard deviation) of the ten calculated-to-observed ^{83}Kr production rates is 0.82 (±0.27). The worse agreements are for samples 14066,21,2.01 and 67075,8. The Zr abundance used for 14066,21,2.01 is much lower than that for 14066,31,1 (which had better agreement of its predicted and observed ^{83}Kr production rates). The abundances of Zr and especially of Y could be too low for 67075,8. The average predicted-to-observed ^{83}Kr production rate for the other eight samples in Table 3 is 0.92 (±0.19). There could be uncertainties in the chemical abundances used for these samples because these rocks, Apollo 14 or 16 breccias, might not be chemically homogeneous. To insure accurate predictions of noble-gas production rates, it is important that abundances of all major target elements be measured with samples as similar as possible to those used for noble-gas analyses.

Comparisons of the predicted-to-observed isotopic ratios for the ten samples in Table 3 are shown in Fig. 4. The agreements for the $^{78}Kr/^{83}Kr$ ratios are considerably improved relative to those of Hohenberg et al. (1978), the average (and standard deviation) of the predicted-to-observed values being 0.99 (±0.06). The calculated and observed $^{78}Kr/^{83}Kr$ ratios both are low for samples with low Zr/Sr abundance ratios and are high for samples with high Zr/Sr ratios. For the $^{80}Kr/^{83}Kr$ ratios, the averages are 1.14 (±0.17) when Br is included and 0.96 (±0.06) when Br is omitted. For the $^{82}Kr/^{83}Kr$ ratios, the averages with and without Br contributions are 1.12 (±0.05) and 1.07 (±0.04), respectively. As in Hohenberg et al. (1978), the theoretical calculations seem to predict too much ^{80}Kr and ^{82}Kr when neutron-capture reactions with Br are included. The lower observed concentrations of ^{80}Kr and ^{82}Kr could be due to partial loss of neutron-capture-produced Kr at the temperatures of the lunar surface or to leachable Br components (Reed and Jovanovic, 1971). Losses of neutron-capture-produced Xe were observed by Hohenberg and Reynolds (1969) for neutron-irradiated samples of meteorites. Marti et al. (1973) have pointed out that Br(n,γ) reactions are not important contributors of spallogenic ^{80}Kr and ^{82}Kr in most lunar rocks. Generally the Br contributions to ^{80}Kr and ^{82}Kr are not important for rocks with simple exposure histories near the lunar surface. To show the differences due to including or omitting Br in the calculations, the $^{80}Kr/^{83}Kr$ and $^{82}Kr/^{83}Kr$ comparisons in Fig. 4 are plotted both with and without Br contributions.

The predicted-to-observed $^{81}Kr/^{83}Kr$ ratios averaged 1.11 (±0.07) for the ten well-documented samples of Table 3. The biggest spread in this comparison of predicted and observed ratios is for $^{84}Kr/^{83}Kr$, the average and standard deviations being 1.13 ± 0.34. (If the four samples with the worse agreements are omitted, the average is 1.01 ± 0.10.) The amounts of the disagreements show no strong correlations with chemical variations, although generally the $^{84}Kr/^{83}Kr$ ratios are slightly overpredicted for samples with high Zr abundances. Much of this spread is probably due to uncertainties in determining the cosmogenic components, especially in samples like 68815,113 which have short exposure ages. The predicted $^{86}Kr/^{83}Kr$ ratios range from 0.0064 to 0.0124, lower than the 0.015 value adopted for cosmogenic Kr. However, as noted above, the $Zr(p,x)^{86}Kr$ excitation function is very uncertain, especially for contributions from isotopes heavier than ^{90}Zr.

A study was made for the ten samples in Table 3 to see if variations in the ratio $(^{m}Kr/^{83}Kr)_{predicted} / (^{m}Kr/^{83}Kr)_{observed}$ correlated with differences in sample chemistries, shielding depths, or exposure ages. Generally the correlations were weak. The best correlation was the predicted-to-observed $^{84}Kr/^{83}Kr$ ratios decreasing with increasing exposure ages. Sample 68815,113 (the only one with a 2 m.y. exposure age) dominated this trend and, when this sample was omitted in the comparison, the absolute value of the correlation coefficient was much smaller (-0.62), although still one of the largest found in this study. The absence of strong correlations indicates that relative production ratios calculated for different chemistries and depths in lunar rocks with simple exposure histories should be good.

Table 4 presents comparisons of Kr isotopic ratios for the three bulk lunar samples with unknown irradiation histories used by Hohenberg <u>et al</u>. (1978) and for the three ilmenite separates given in Table 2. For the bulk samples of the Apollo 11 rocks given in Table 2 but not here, the range of predicted isotopic ratios would be similar to those for rock 10044 in Table 4. The observed $^{78}Kr/^{83}Kr$ and $^{80}Kr/^{83}Kr$ ratios are all within the ranges of the predicted ratios calculated for lunar depths of 10 and 500 g/cm^2. All the observed $^{82}Kr/^{83}Kr$ ratios are lower than the predicted range and the observed $^{84}Kr/^{83}Kr$ ratios are higher than predictions. These trends for agreements or disagreements of observed and predicted Kr isotopic ratios generally are similar to those for the data in Table 3.

The cosmogenic $^{78}Kr/^{83}Kr$ ratios of the ilmenite separates of the three Apollo 11 rocks presented in Table 2 were used to infer their effective shielding depths in the moon. These depths and the predicted isotopic ratios for the bulk samples and ilmenite separates are given in Table 5 for these rocks. For Zr as a target, the predicted $^{78}Kr/^{83}Kr$ is 0.223 at the surface, increases to about 0.26 near 10 g/cm^2, is 0.223 again at a depth of about 135 g/cm^2, and becomes 0.186 below 500 g/cm^2 (see Fig. 3). Thus for $^{78}Kr/^{83}Kr$ ratios above 0.223, there are two possible depths. For rocks 10017 and 10071, their average effective depths could be near the surface or at the depths given in Table 5. Because the $^{131}Xe/^{126}Xe$ ratio increases monotonically from about 3 at the surface to around 19 below 500 g/cm^2 (Hohenberg et al., 1978), it was used to eliminate near-surface exposures for rocks 10017 and 10071 (which had $^{131}Xe/^{126}Xe$ ratios of 8.0 and 5.8, respectively). These $^{131}Xe/^{126}Xe$ ratios are consistent with the inferred depths for these two rocks. The $^{80}Kr/^{83}Kr$ ratios calculated for these deeper burial depths agree with the observed ilmenite ratios. The predicted total-rock $^{78}Kr/^{83}Kr$ ratios also agree with the measured values for these two rocks.

The ilmenite separate for rock 10047 implies an effective shielding depth of 15 ± 10 g/cm^2. However, the measured $^{131}Xe/^{126}Xe$ ratio of 4 and the observed ilmenite $^{80}Kr/^{83}Kr$ ratio correspond to depths around 60 to 80 g/cm^2. Also the total-rock $^{78}Kr/^{83}Kr$ calculated for this shallow depth is 1.125 times greater than the observed ratio, well outside any predicted-to-observed ratio from

Table 3. The observed total-rock $^{78}Kr/^{83}Kr$ ratio for this rock implies a depth of 81 ± 10 g/cm^2, much more consistent with the $^{131}Xe/^{126}Xe$ and ilmenite $^{80}Kr/^{83}Kr$ ratios than a depth of 15 ± 10 g/cm^2. We believe that this deeper depth is probably closer to the truth, although it is possible that this rock's history is so complex that no one effective shielding depth would be consistent with all cosmogenic noble-gas ratios. In Table 5 for rock 10047, we present predicted isotopic ratios for both depths.

For both the ilmenite separates (in which Zr is the only major target for producing Kr isotopes) and the bulk samples, the predicted $^{82}Kr/^{83}Kr$ and $^{84}Kr/^{83}Kr$ ratios are higher and lower, respectively, than the observed ones. The predicted $^{82}Kr/^{83}Kr$ ratios are about 10% higher than measured, similar to the differences observed in Tables 3 and 4. The predicted $^{84}Kr/^{83}Kr$ ratios are about 0.76 of the observed ones, about the same as the differences observed in Table 4, but less than the better agreement for the data in Table 3. The rocks in Table 3 have poorly defined cosmogenic ^{84}Kr contents and shallow shielding depths, whereas those in Tables 4 and 5 have better defined cosmogenic ^{84}Kr contents and deeper effective shielding depths. Thus the reason for the relatively better predicted-to-observed agreements for $^{84}Kr/^{83}Kr$ in Table 3 and the worse predictions of this ratio in other rocks is not clear. If the calculated and observed $^{84}Kr/^{83}Kr$ ratios disagree more at depth than near the surface, then the shapes of the excitation functions are wrong, having cross sections which are too high at high energies and/or too low at low energies. As mentioned above, the samples compared in Table 3 had relatively short exposure ages, and too much trapped and/or fission-produced ^{84}Kr could have been removed in determining their spallogenic ^{84}Kr component.

Summary and Conclusions

Theoretical cosmic-ray production rates and isotopic ratios for Kr have been compared with those determined from lunar-sample measurements to delineate areas of agreement and disagreement and to define areas where future work is most appropriate. Since the calculations and comparisons presented in Hohenberg et al. (1978) were made, additional excitation functions for Kr production became available and Kr in ilmenite separates from several Apollo 11 rocks has been analyzed. However, there is a need for additional cross-section measurements and for more cosmogenic-noble-gas and target-element-abundance measurements on a variety of lunar rocks and mineral separates.

In general, the agreements of calculated and observed production rates and ratios were quite good; differences seldom exceeded 20%. There was considerable scatter in calculated-to-observed ^{83}Kr production rates, possibly due in part to poorly known abundances for the target elements. The very good agreements for the ^{78}Kr/^{83}Kr ratios in samples with different shielding depths and a variety of chemical abundances gives us confidence that the predictive systematics are good enough for use in unfolding the records of samples with complex exposure histories (e.g., Eugster et al., 1979). The observed ^{78}Kr/^{83}Kr ratios of bulk samples and ilmenite separates for three Apollo 11 rocks were used to determine effective shielding depths that are in accord with other noble-gas isotopic ratios. The ^{80}Kr/^{83}Kr and ^{82}Kr/^{83}Kr ratios suggest that much of the Br(n,γ)-produced Kr in lunar rocks is lost and thus such Br contributions are less than calculated. The ^{80}Kr/^{83}Kr ratios calculated without Br contributions agree well with observed ratios. The predicted ^{81}Kr/^{83}Kr and ^{82}Kr/^{83}Kr ratios tended to be about 10% greater than the observed ratios. There are no indications from these comparisons of any serious errors in the systematics used to determine ^{81}Kr-^{83}Kr exposure ages. There was a considerable spread in the calculated-to-observed cosmogenic $^{84}Kr/^{83}Kr$ ratios, probably due to uncertainties in correcting for trapped or fission components of ^{84}Kr and/or in the excitation functions for ^{84}Kr production. All five target elements (Br, Rb, Sr, Y, and Zr) can make significant contributions to at least several Kr isotopes. Production by solar cosmic rays and effects of erosion are important for samples which were within a few g/cm^2 of the lunar surface.

While the predictive systematics, especially for ^{78}Kr, ^{80}Kr, and ^{84}Kr are better than those of Hohenberg et al. (1973), there is room for improvement. Experimental excitation functions at all energies for the Sr(p,x)Kr and Zr(p,x)Kr reactions probably would make the calculated production rates agree better with observations. Some cross sections measured with incident neutrons might help improve the theoretical rates for the production of the heavier Kr isotopes by low-energy GCR secondary particles. The observational data base could be expanded by additional measurements on well-documented samples and on mineral separates. Better chemical abundance data are needed for samples used in noble-gas analyses. The excitation functions for the production of Kr isotopes now are more than adequate for predicting Kr systematics in meteorites using flux models such as those of Reedy et al. (1979). The Kr predictive production systematics are good enough that they should be used along with those for Xe (Hohenberg et al., 1978) in studies of lunar samples with complex exposure histories.

ACKNOWLEDGEMENTS

We gratefully acknowledge the assistance of L. Wagoner in preparation of this manuscript. This work was supported in part by NASA grants NSG-07-016 and NSG-05-009-150 and NASA Work Order W-14,084.

REFERENCES

Annell C. S. and Helz A. W. (1970) Emission spectrographic determination of trace elements in lunar samples from Apollo 11. Proc. Apollo 11 Lunar Sci. Conf., p. 991-994.

Caretto A A. and Wiig E. O. (1956) Spallation of yttrium by 240-MeV protons. Phys. Rev. 103, 236-239.

Caretto A. A. and Wiig E. O. (1959) Spallation of yttrium with protons of energy between 60 and 240 MeV. Phys. Rev. 115, 1238-1243.

Compston W., Chappell B. W., Arriens P. A. and Vernon M. J. (1970) The chemistry and age of Apollo 11 lunar material. Proc. Apollo 11 Lunar Sci. Conf., p. 1007-1027.

Crozaz G., Drozd R., Hohenberg C. M., Hoyt H. P. Jr., Ragan D., Walker R. M. and Yuhas D. (1972) Solar flare and galactic cosmic ray studies of Apollo 14 and 15 samples. Proc. Lunar Sci. Conf. 3rd, p. 2917-2931.

Eberhardt P., Geiss J., Graf H., Grögler N., Mendia M. D., Mörgeli M., Schwaller H., Stettler A., Krähenbühl U. and von Gunten H. R. (1972) Trapped solar wind noble gases in Apollo 12 lunar fines 12001 and Apollo 11 breccia 10046. Proc. Lunar Sci. Conf. 3rd, p. 1821-1856.

Eberhardt P., Geiss J., Graf H., Grögler N., Krähenbühl U., Schwaller H. and Stettler A. (1974) Noble gas investigations of lunar rocks 10017 and 10071. Geochim. Cosmochim. Acta 38, 97-120.

Eugster O., Eberhardt P., Geiss J. and Grögler N. (1979) History of black and orange soil from drive tubes 74001 and 74002 (abstract). In Lunar and Planetary Science X, p. 367-369. Lunar and Planetary Institute, Houston.

Funk H., Podosek F. and Rowe M. W. (1967) Spallation yields of krypton and xenon from irradiation of strontium and barium with 730 MeV protons. Earth Planet. Sci. Lett. 3, 193-196.

Gast P. W., Hubbard N. J. and Wiesmann H. (1970) Chemical composition and petrogenesis of basalts from Tranquillity Base. Proc. Apollo 11 Lunar Sci. Conf., p. 1143-1163.

Goles G. G., Randle K., Osawa M., Schmitt R. A., Wakita H., Ehmann W. D. and Morgan J. W. (1970) Elemental abundances by instrumental activation analyses in chips from 27 lunar rocks. Proc. Apollo 11 Lunar Sci. Conf., p. 1165-1176.

Hohenberg C. M., Marti K., Podosek F. A., Reedy R. C. and Shirck J. R. (1978) Comparisons between observed and predicted cosmogenic noble gases in lunar samples. Proc. Lunar Planet. Sci. Conf. 9th, p. 2311-2344.

Hohenberg C. M. and Reynolds J. H. (1969) Preservation of the iodine-xenon record in meteorites. J. Geophys. Res. 74, 6679-6683.

Korteling R. G. and Hyde E. K. (1964) Interaction of high-energy protons and helium ions with niobium. Phys. Rev. 136, B425-B437.

Lingenfelter R. E., Canfield E. H. and Hampel V. E. (1972) The lunar neutron flux revisited. Earth Planet. Sci. Lett. 16, 355-369.

Marti K., Eberhardt P. and Geiss J. (1966) Spallation, fission and neutron capture anomalies in meteoritic krypton and xenon. Z. Naturforschg. 21a, 398-413.

Marti K., Lightner B. D. and Osborn T. W. (1973) Krypton and xenon in some lunar samples and the age of North Ray crater. Proc. Lunar Sci. Conf. 4th, p. 2037-2048.

Marti K. and Lugmair G. W. (1971) Kr^{81}-Kr and K-Ar^{40} ages, cosmic-ray spallation products, and neutron effects in lunar samples from Oceanus Procellarum. Proc. Lunar Sci. Conf. 2nd, p. 1591-1605.

Marti K., Lugmair G. W. and Urey H. C. (1970) Solar wind gases, cosmic-ray spallation products and the irradiation history of Apollo 11 samples. Proc. Apollo 11 Lunar Sci. Conf. p. 1357-1367.

Maxwell J. A., Peck L. C. and Wiik H. B. (1970) Chemical composition of Apollo 11 samples 10017, 10020, 10072, and 10084. Proc. Apollo 11 Lunar Sci. Conf., p. 1369-1374.

Morrison D. and Caretto A. A. (1962) Excitation functions of (p,xp) reactions. Phys. Rev. 127, 1731-1738.

Porile N. T., Tanaka S., Amano H., Furukawa M., Iwata S. and Yagi M. (1963) Nuclear reactions of ^{69}Ga and ^{71}Ga with 13-56 MeV protons. Nuclear Phys. 43, 500-522.

Reed G. W., Jr., and Jovanovic S. (1970) Halogens, mercury, lithium and osmium in Apollo 11 samples. Proc. Apollo 11 Lunar Sci. Conf., p. 1487-1492.

Reed G. W. and Jovanovic S. (1971) The halogens and other trace elements in Apollo 12 samples and the implications of halides, platinum metals, and mercury on surfaces. Proc. Lunar Sci. Conf. 2nd, p. 1261-1276.

Reedy R. C. and Arnold J. R. (1972) Interaction of solar and galactic cosmic ray particles with the moon. J. Geophys. Res. 77, 535-555.

Reedy R. C., Herzog G. F. and Jessberger E. K. (1979) The reaction Mg(n,α)Ne at 14.1 and 14.7 MeV: Cross sections and implications for meteorites. Earth Planet. Sci. Lett., to be published.

Regnier S. (1979) Production of Kr isotopes by spallation on Y targets and implications for Kr-Kr dating (abstract). In Lunar and Planetary Science X, p. 1013-1015. Lunar and Planetary Institute, Houston.

Remsberg L. P. and Miller J. M. (1963) Study of (p,pn) reactions in medium weight nuclei at 370 MeV. Phys. Rev. 130, 2069-2076.

Rudstam G. and Bruninx E. (1961) Spallation of arsenic with 590 MeV protons. J. Inorg. Nucl. Chem. 23, 161-165.

Sachdev D. R., Porile N. T. and Yaffe L. (1967) Reactions of ^{88}Sr with protons of energies 7 to 85 MeV. Can. J. Chem. 45, 1149-1160.

Strohal P. P. and Caretto A. A. (1961) Excitation functions of (p,2 nucleon) reactions. Phys. Rev. 121, 1815-1822.

Ünseren E. and Wiig E. O. (1961) Excitation functions of the (p,2p6n) and (p,3p5n) reactions for 60-, 100-, 150-, and 240-MeV protons on enriched ^{90}Zr. Phys. Rev. 122, 1875-1876.

Wahlen M., Honda M., Imamura M., Fruchter J. S., Finkel R. C., Kohl C. P., Arnold J. R. and Reedy R. C. (1972) Cosmogenic nuclides in football-sized rocks. Proc. Lunar Sci. Conf. 3rd, p. 1719-1732.

Woolum D. S., Burnett D. S., Furst M. and Weiss J. R. (1975) Measurement of the lunar neutron density profile. The Moon 12, 231-250.

Yuhas D. (1974) The particle track record in lunar silicates: Long term behavior of solar and galactic VH nuclei and lunar surface dynamics. Ph.D. thesis, Washington University, St. Louis, Missouri.

TABLE 1. Predicted Cosmogenic Production Rate [a] for Krypton Isotopes in the Moon, in units of atoms/min/kg(element).

M	Rb	Sr	Y	Zr	Br
		Surface			
78	6.4 + 7.5	12.6 + 4.2	24.9 + 4.8	20.4 + 4.3	0
80	74.5 + 263	34.9 + 12.1	57.2 + 15.7	44.7 + 10.2	5710
81	66.8 + 232	44.1 + 35.8	65.2 + 43.9	51.3 + 23.3	0
82	122 + 986	52.8 + 67.4	81.5 + 118	61.2 + 47.9	2470
83	98.8 + 1302	64.5 + 161	96.9 + 67.0	72.0 + 38.9	0
84	163 + 1641	30.6 + 135	22.9 + 36.7	19.8 + 9.7	0
86	9.3 + 30.1	0.92 + 1.63	.070 + .003	0.41 + 0.53	0
		1 g/cm^2 Shielding			
78	6.5 + 4.7	12.7 + 2.9	25.0 + 3.5	20.5 + 3.1	0
80	75.6 + 115	35.0 + 8.4	57.3 + 11.2	44.8 + 7.4	6400
81	67.9 + 104	44.4 + 23.2	65.5 + 26.0	51.5 + 16.0	0
82	125 + 343	53.3 + 39.4	82.2 + 61.6	61.7 + 30.5	2770
83	102 + 414	65.4 + 73.9	97.6 + 44.2	72.5 + 26.6	0
84	167 + 423	31.1 + 52.5	23.0 + 18.0	19.9 + 6.3	0
86	9.4 + 11.9	0.92 + 0.71	.070 + .002	0.41 + 0.31	0
		2 g/cm^2 Shielding			
78	6.6 + 3.5	12.7 + 2.2	25.0 + 2.8	20.5 + 2.5	0
80	76.8 + 74.4	35.2 + 6.6	57.5 + 8.9	45.0 + 6.0	7089
81	69.1 + 68.9	44.8 + 17.6	65.9 + 19.1	51.8 + 12.5	0
82	128 + 206	53.9 + 28.5	82.9 + 43.0	62.1 + 22.9	3069
83	105 + 234	66.4 + 48.9	98.4 + 33.8	73.1 + 20.7	0
84	171 + 237	31.5 + 32.7	23.2 + 12.0	19.9 + 4.8	0
86	9.5 + 7.6	0.93 + 0.46	.069 + .002	0.41 + 0.22	0
		5 g/cm^2 Shielding			
78	6.9 + 1.9	12.7 + 1.3	25.1 + 1.8	20.6 + 1.5	0
80	80.7 + 32.6	35.6 + 3.9	58.1 + 5.4	45.4 + 3.7	9180
81	73.0 + 31.1	46.1 + 9.6	67.1 + 10.3	52.8 + 7.3	0
82	138 + 79.5	55.8 + 14.5	85.4 + 21.0	63.6 + 12.4	3970
83	116 + 81.2	69.6 + 22.3	101 + 18.9	74.8 + 12.0	0
84	183 + 86.0	33.0 + 13.4	23.6 + 5.4	20.1 + 2.6	0
86	9.9 + 3.2	0.94 + 0.20	.067 + .001	0.42 + 0.11	0
		10 g/cm^2 Shielding			
78	7.3 + 0.9	12.8 + 0.7	25.2 + 1.0	20.7 + 0.9	0
80	86.5 + 13.6	36.2 + 2.1	58.7 + 2.9	45.9 + 2.1	12650
81	78.7 + 13.3	47.5 + 4.8	68.6 + 5.1	54.0 + 3.8	0
82	153 + 29.8	58.4 + 6.7	88.8 + 9.5	65.7 + 6.0	5480
83	132 + 28.1	74.2 + 9.7	105 + 9.5	77.2 + 6.2	0
84	203 + 31.8	35.3 + 5.3	24.3 + 2.3	20.3 + 1.3	0
86	10.4 + 1.3	0.96 + 0.08	.065 + .001	0.44 + 0.05	0
		20 g/cm^2 Shielding			
78	7.7 + 0.3	12.6 + 0.3	24.8 + 0.4	20.5 + 0.4	0
80	94.1 + 4.3	36.5 + 0.8	58.6 + 1.2	45.8 + 0.9	18100
81	86.2 + 4.2	49.8 + 1.7	69.8 + 1.9	54.8 + 1.5	0
82	174 + 8.5	61.4 + 2.3	92.6 + 3.3	67.6 + 2.2	7840
83	156 + 7.3	79.8 + 3.3	108 + 3.5	79.3 + 2.4	0
84	231 + 9.0	38.3 + 1.6	24.9 + 0.8	20.3 + 0.5	0
86	11.1 + 0.4	0.98 + 0.03	.061 + .000	0.46 + 0.02	0

M	Rb	Sr	Y	Zr	Br
		40 g/cm^2 Shielding			
78	7.7	11.6	22.6	18.7	0
80	97.1	34.0	54.1	42.1	29500
81	89.6	43.4	66.0	51.7	0
82	169	60.6	90.6	65.0	12800
83	177	81.0	104	75.8	0
84	252	39.4	24.0	18.9	0
86	11.1	0.93	.052	0.44	0
		65 g/cm^2 Shielding			
78	7.1	9.9	19.2	15.9	0
80	91.5	29.5	46.6	36.1	42400
81	84.9	43.4	58.1	45.3	0
82	186	55.0	82.0	57.9	18400
83	178	75.2	93.0	67.2	0
84	247	37.2	21.5	16.4	0
86	10.3	0.83	.042	0.40	0
		100 g/cm^2 Shielding			
78	5.8	7.7	14.7	12.3	0
80	77.4	23.1	36.1	28.0	53300
81	72.1	35.1	45.1	35.8	0
82	163	45.0	66.8	46.5	23100
83	160	62.6	74.6	53.5	0
84	217	31.6	17.4	12.8	0
86	8.6	0.67	.031	0.33	0
		150 g/cm^2 Shielding			
78	4.3	5.4	10.1	8.5	0
80	60.3	16.3	25.2	19.4	52900
81	56.4	25.7	33.1	25.6	0
82	132	33.6	49.7	33.9	22900
83	133	47.8	54.4	38.6	0
84	176	24.7	12.9	9.1	0
86	6.6	0.49	.020	0.24	0
		225 g/cm^2 Shielding			
78	2.85	3.23	5.9	5.0	0
80	41.9	9.8	15.0	11.5	44500
81	39.2	16.4	20.6	15.7	0
82	97.0	21.9	32.5	21.5	19300
83	101	32.1	34.4	24.1	0
84	130	17.3	8.4	5.6	0
86	4.5	0.32	.011	0.16	0
		500 g/cm^2 Shielding			
78	0.41	0.40	0.69	0.59	0
80	6.78	1.23	1.84	1.38	6160
81	6.35	2.29	2.75	2.04	0
82	17.1	3.20	4.75	2.98	2670
83	18.5	4.92	4.69	3.18	0
84	22.9	2.87	1.24	0.73	0
86	0.72	.048	.001	.024	0

[a]The first column, M, is the mass of the Kr isotope. Rates are for spallation reactions induced by GCR particles. Second entries [illegible] shallow depths are rates for reactions by solar [illegible] tions.

Table 2. Isotopic Composition and Concentration of Bulk and Spallogenic Krypton in Total Samples and Ilmenite Separates for Several Apollo 11 Rocks.

	78	80	81	82	83	84	86	83 conc. $x10^{-12}$ cm^3STP/g
10017,56 TR (a)	16.64	47.[illegible]	0.0385	75.8	= 100	58.2	6.38	950 ± 140
	.21	.5	.0019	.4		.5	.10	
same - spall.	17.09	48.8	0.0398	75.0	= 100	43.6	= 1.53	920
	.21	.5	.0019	.4		1.0	.10	
10017,56 Ilmenite (b)	20.57	48.4	0.040	78.6	= 100	64.1	13.38	810 ± 150
	.41	1.3	.005	.6		.5	.40	
same - spall.	22.1	50.9	0.043	76.8	= 100	27.4	= 1.5	747
	.5	1.4	.005	.8		1.0		
10047,40 (a)	18.42	49.5	0.202	77.4	= 100	67.2	9.27	160 ± 25
	.22	.4	.009	.4		.5	.20	
same - spall.	19.24	51.1	0.213	76.2	= 100	43.9	= 1.55	152
	.23	.4	.009	.4		1.0	.20	
10047,40 Ilmenite (b)	16.80	40.2	0.136	87.0	= 100	212.5	60.4	240 ± 40
	.25	.5	.010	1.3		1.4	1.0	
same - spall.	25.7	53.5	0.224	78.6	= 100	31.3	= 1.5	146
	.4	.8	.017	2.1		2.3		
10071 .R (c)								
Ave. spall.	18.97	51.4	0.052	76.5	= 100	41.7	= 1.5	926
	.25	.5	.002	.5		1.1		
10071 Ilmenite (c) spall.	22.7	53.9	0.055	76.2	= 100	32.9	= 1.5	646
	1.1	3.0	.007	4.1		2.4		
10071 Feldspar (c) ave. spall.	17.15	49.3	0.052	75.4	= 100	50.0	= 1.5	1520
	.25	.6	.006	.7		4.0		

(a) Marti et al. (1970)

(b) La Jolla data, this work.

(c) Data from Eberhardt et al. (1974).

Table 3. Comparisons of Observed and Predicted Cosmogenic Kr in Lunar Rocks with Known Exposure Histories[a].

Sample / Shielding Depth / Exposure Age	Target Chemistry (ppm)	$\frac{^{83}Kr_c \text{ (measured)}}{^{83}Kr_c \text{ (predicted)}}$[b] ($\times10^{-12}$ cm³STP/g m.y.)	Cosmogenic ratios (^{83}Kr≡100)			
				Observed	Predicted[c,e]	Predicted[d,e]
			78	23.4 (2)	23.0 (5)	23.1 (5)
			80	53.0 (4)	57.7 (8)	57.5 (8)
14066,21,2.01	6.19 Rb	3.58 (20)			54.5 (6)	54.6 (6)
	180 Sr		81	0.70(1)	0.73(1)	0.73(1)
10 g/cm^2	115 Y	1.46	82	77.6 (8)	86.0 (5)	86.0 (4)
	550 Zr	[1.47]			84.6 (4)	84.7 (4)
27.8 m.y.	0.168 Br		84	24.0 (10)	31.5 (11)	31.6 (11)
			86	=1.5	0.71(4)	0.72(4)
			78	23.1 (4)	23.4 (4)	23.5 (5)
			80	52.6 (7)	57.7 (5)	57.6 (4)
14066,31,1	26 Rb	3.55 (20)			55.6 (4)	55.8 (4)
	150 Sr		81	0.70(3)	0.74(1)	0.74(1)
10 g/cm^2	200 Y	2.31	82	76.7 (14)	86.9 (4)	86.9 (4)
	950 Zr	[2.32]			86.0 (3)	86.2 (3)
27.7 m.y.	0.168 Br		84	25.0 (36)	32.0 (14)	32.0 (13)
			86	=1.5	0.79(6)	0.79(6)
			78	26.4 (15)	23.2 (5)	23.0 (5)
			80	53.6 (36)	57.7 (6)	56.8 (6)
14306,26L	32 Rb	2.31 (35)			55.3 (5)	54.8 (5)
	230 Sr		81	0.73(7)	0.82(1)	0.80(1)
7 g/cm^2	148 Y	2.71	82	85.4 (52)	87.2 (4)	87.5 (4)
	1150 Zr	[2.77]			86.1 (3)	86.6 (4)
25.4 m.y.	0.27 Br		84	31.8 (74)	33.5 (16)	33.9 (16)
			86	=1.5	0.87(7)	0.89(7)

Table 3, cont.

			78	23.9 (8)	23.9 (4)	23.7 (4)
			80	57.7 (21)	57.5 (5)	56.7 (5)
14306,26D	14 Rb	4.21 (63)			55.4 (4)	55.0 (4)
	195 Sr		81	0.77(4)	0.89(1)	0.87(1)
7 g/cm^2	297 Y	3.29	82	79.0 (27)	86.7 (3)	87.2 (3)
	1370 Zr	[3.36]			85.9 (2)	86.5 (2)
23.4 m.y.	0.27 Br		84	27.0 (38)	29.3 (8)	29.7 (8)
			86	=1.5	0.64(3)	0.65(3)
			78	23.6 (2)	22.0 (5)	19.6 (7)
			80	53.4 (4)	55.3 (7)	49.3 (8)
14171,2	26 Rb	2.75 (41)			52.7 (5)	47.7 (8)
	150 Sr		81	0.74(2)	0.91(1)	0.77(1)
1 g/cm^2	200 Y	2.59	82	78.7 (7)	89.5 (5)	91.5 (8)
	950 Zr	[3.07]			88.4 (4)	90.8 (8)
24.5 m.y.	0.39 Br		84	30.3 (5)	34.5 (17)	38.8 (23)
			86	=1.5	0.86(7)	0.95(7)
			78	20.8 (2)	21.6 (6)	21.2 (6)
			80	51.9 (2)	57.5 (13)	54.7 (10)
67095,9	6.0 Rb	0.78 (12)			52.9 (7)	51.8 (8)
	150 Sr		81	0.37(1)	0.42(1)	0.39(1)
5 g/cm^2	61 Y	0.82	82	78.1 (1)	86.1 (7)	86.2 (7)
	250 Zr	[0.86]			84.1 (5)	84.9 (7)
50.2 m.y.	0.14 Br		84	49.1 (5)	35.4 (15)	36.4 (16)
			86	=1.5	0.86(6)	0.88(6)
			78	21.1 (7)		21.9 (6)
			80	58.7 (20)		78.4 (60)
68815,113	8.8 Rb	1.17 (18)			(f)	53.5 (7)
	160 Sr		81	10.0 (4)		10.0 (7)
18 g/cm^2	64.4 Y		82	82.5 (31)		94.9 (27)
	331 Zr	(f)				84.1 (5)
2 m.y.	0.72 Br	[0.96]	84	18. (5)		34.8 (16)
			86	=1.5		0.87(6)

Table 3, Cont.

			78	21.8 (7)	21.3-21.6(6)	18.1-19.7(7)
			80	56.6 (10)	61.0-62.5(25)	48.2-52.8(16)
67015,14	3.0 Rb	1.21 (18)			51.4-52.1(8)	44.0-47.5(12)
	150 Sr		81	0.38(3)	0.45-0.43(1)	0.35-0.37(1)
1-2 g/cm^2	87 Y	0.93-0.91	82	78.4 (9)	88.7-88.9(13)	87.4-87.9(15)
	260 Zr	[1.18-1.06]			84.5-84.4(7)	85.5-85.7(15)
51.1 m.y.	0.4 Br		84	35.7 (15)	34.5-33.9(15)	40.7-37.5(19)
			86	=1.5	0.75-0.74(5)	0.83-0.79(5)
			78	15.0 (6)	15.8-16.2(2)	13.4-16.6(2)
			80	50.8 (11)	70.3-84.7(99)	49.3-75.6(64)
67075,8	0.67 Rb	0.53 (8)			44.4-46.0(3)	37.4-46.6(3)
	127 Sr		81	0.37(4)	0.42-0.36(1)	0.33-0.38(1)
2-10 g/cm^2	1.4 Y	0.24-0.22	82	75.1 (16)	88.5-94.7(44)	78.2-91.2(29)
	7.6 Zr	[0.31-0.23]			77.3-77.9(3)	73.0-78.6(3)
50.2 m.y.	0.265 Br		84	52.9 (65)	49.3-47.5(4)	54.9-47.7(4)
			86	=1.5	1.24-1.23(1)	1.22-1.25(1)
			78	25.0 (1)	23.0 (4)	23.2 (4)
			80	57.6 (2)	59.9 (12)	59.7 (11)
14321,92,FM-3D	15.7 Rb	1.96 (29)			50.7 (6)	51.0 (6)
	188 Sr		81	0.70(2)	0.82(1)	0.81(1)
18 g/cm^2	216 Y	2.25	82	81.2 (3)	87.2 (6)	87.1 (6)
	700 Zr	[2.27]			84.1 (7)	84.2 (7)
25 m.y.	0.317 Br		84	34.8 (6)	30.7 (11)	30.7 (11)
			86	=1.5	0.70(5)	0.70(5)

[a]See Hohenberg et al. (1978) for sources of chemical and Kr data. Quantities in parentheses are uncertainties of last digit(s), e.g., 3.58 (20) is 3.58 ± 0.20. Uncertainties for the predicted ratios are those from 20% uncertainties in elemental abundances. For rocks 67015 and 67075, results for two depths are given.

[b]Predicted rates are with 0.3 g/cm^2/m.y. and, in [], no erosion. Uncertainties are ±20% for predicted rates.

[c]Calculated assuming an erosion rate of 0.3 g/cm^2/m.y.

[d]Calculated assuming no erosion.

[e]Lower set of rates for ^{80}Kr and ^{82}Kr are predicted assuming no Br.

[f]Same as for no erosion.

Table 4. Comparisons of Observed and Predicted Isotopic Ratios of Cosmogenic Kr in Lunar Rocks with Unknown Irradiation Histories.[(a)]

Sample $^{86}Kr/^{78}Kr$	Target Chemistry (ppm)		Cosmogenic Ratios (^{83}Kr=100)		Predicted[(b)]	
				Observed	10 g/cm^2	500 g/cm^2
			78	17.5(2)	21.5(6)	12.9(6)
12021,61	1.2	Rb	80	50.7(5)	53.6(7)	44.2(27)
	100	Sr			52.6(7)	34 2(11)
	50	Y	82	76.2(4)	83.8(5)	87.0(24)
	115	Zr			83.4(5)	82.7(20)
0.09	0.018	Br	84	49.9(44)	34.2(14)	41.3(22)
			86	≈1.5	0.75(5)	0.75(4)
			78	16.7(1)	20.6(6)	11.9(6)
15475,135	0.73	Rb	80	49.7(4)	65.8(36)	175(36)
	117	Sr			51.4(8)	32.2(11)
	29	Y	82	75.6(5)	89.5(17)	141(16)
0.13	82	Zr			82.2(6)	78.4(20)
	0.235	Br	84	54.8(5)	36.8(16)	45.0(23)
			86	≈1.5	0.85(5)	0.81(3)
			78	18.3(5)	22.9(5)	14.4(5)
10044,20	5.64	Rb	80	48.6(10)	58.2(9)	79.3(98)
	167	Sr			54.4(5)	37.3(9)
	167	Y	82	78.7(5)	86.4(5)	106.3(45)
	460	Zr			84.8(3)	88.1(15)
1.07	0.216	Br	84	40.2(5)	31.1(11)	36.2(20)
			86	≈1.5	0.66(5)	0.72(4)
			78	22.1-25.7	25.9	18.5
			80	50.9-53.9	57.6	43.2
Ilmenite	~2000	Zr				
			82	76.2-78.6	86.0	93.7
(c)						
			84	27.4-32.9	25.9	22.8
			86	≈1.5	0.59	0.74

[a]See Hohenberg et al. (1978) for sources of chemical and Kr isotopic data for first three samples. Quantities in parentheses are uncertainties of last digit(s), e.g. 17.5(2) is 17.5 ± 0.2. Uncertainties for the predicted ratios are those from 20% uncertainties in elemental abundances.

[b]Lower set of notes for ^{80}Kr and ^{82}Kr are predicted assuming no Br.

[c]Ranges of observed cosmogenic ratios are given for the three ilmenite separates of Table 2.

Table 5. Comparisons of Observed and Predicted Isotopic Ratios of Cosmogenic Kr in Bulk Samples and Ilmenite Separates of Apollo 11 Rocks with Effective Shielding Depths Inferred from Observed $^{78}Kr/^{83}Kr$ Ratios [a].

Sample Effective Shielding Depth	Target Chemistry (ppm)			Cosmogenic Ratios (^{83}Kr≡100) Total Rock Observed	Total Rock Predicted[b]	Ilmenite Separate Observed	Ilmenite Separate Predicted
			78	17.1(2)	18.4 (6)	22.1(5)	≡22.1
	5.6	Rb	80	48.8(5)	57.2 (27)	50.9(14)	50.7
10017,56	167	Sr			45.9 (9)		
	160	Y	82	75.0(4)	89.7 (16)	73.8(8)	87.7
142 ± 20 g/cm^2	430	Zr			84.8 (8)		
	0.077	Br	84	43.6(10)	32.5 (15)	27.4(10)	23.6
	(c,d)		86	=1.5	0.67(4)	=1.5	0.62
			78	19.2(2)	≡19.2 (6) [21.6 (4)]	25.7(4)	23.4 [≡25.7]
	1.1	Rb	80	51.1(4)	58.8 (27) [55.8 (26)]	53.5(8)	53.2 [57.3]
10047,40	209	Sr			47.6 (8) [53.0 (13)]		
	134	Y	82	76.2(4)	87.6 (14) [84.6 (8)]	78.6(21)	86.5 [85.7]
81 ± 10 g/cm^2	334	Zr			82.8 (8) [83.4 (12)]		
[15 ± 10 g/cm^2]	0.11	Br	84	43.9(10)	32.5 (15) [31.9 (14)]	31.3(23)	24.2 [25.7]
	(d)		86	=1.5	0.64(4) [0.66(2)]	=1.5	0.6 [0.6]
			78	19.0(3)	19.2 (11)	22.7(11)	≡22.7
	5.9	Rb	80	51.4(5)	55.8 (10)	53.9(30)	51.9
10071	165	Sr			47.4 (25)		---
	160	Y	82	76.5(5)	88.3 (20)	76.2(41)	87.1
113 ± 50 g/cm^2	450	Zr			84.7 (4)		---
	0.07	Br	84	41.7(11)	31.9 (5)	32.9(24)	23.9
	(c,e)		86	=1.5	0.66(1)	=1.5	0.61

Table 5, cont.

[a]Quantities in parentheses are uncertainties of last digit(s), e.g., 17.1(2) is 17.1 ± 0.2. Uncertainties for predicted total-rock ratios are based on 20% uncertainties in elemental abundances. Uncertainties in inferred shielding depths are from uncertainties in observed ^{78}Kr/^{83}Kr ratios.

[b]Predicted ratios were calculated assuming no erosion. Lower set of ratios for ^{80}Kr and ^{82}Kr was calculated assuming no Br. The quantities in [] for 10047 are for a different shielding depth (see text).

[c]Cast _et al_. (1970).

[d]Compston _et al_. (1970), Maxwell _et al_. (1970), and Reed and Jovanovic (1970).

[e]Annell and Helz (1970) and Goles _et al_. (1970). The Br concentration is that for 10072 of Reed and Jovanovic (1970).

FIGURE CAPTIONS

Fig. 1. The curves are the excitation functions used here for the production of ^{78}Kr, ^{80}Kr, ^{81}Kr, and ^{82}Kr from targets of rubidium, strontium, yttrium, and zirconium by energetic cosmic-ray particles. The circles are the measured Sr cross sections of Funk <u>et al</u>. (1967) at 0.73 GeV and the crosses are the experimental Y cross sections of Regnier (1979) at 0.08, 0.15, 1.05, and 24 GeV. (The cross sections measured for Y at 24 GeV are shown at an energy of 10 GeV.) The major reaction channels are identified.

Fig. 2. The curves are the excitation functions used here for the production of ^{83}Kr, ^{84}Kr, ^{85}Kr, and ^{86}Kr from targets of rubidium, strontium, yttrium, and zirconium by energetic cosmic-ray particles. The circles are the measured Sr cross sections of Funk <u>et al</u>. (1967) at 0.73 GeV and the crosses are the experimental Y cross sections of Regnier (1979) at 0.08, 0.15, 1.05, and 24 GeV. (The cross sections measured for Y at 24 GeV are shown at an energy of 10 GeV.) The major reaction channels are identified.

Fig. 3. The calculated production ratio $^{78}Kr/^{83}Kr$ as a function of depth in the moon for each of the four main target elements. The changes in these ratios near the surface are caused by solar-proton reactions. The lowering of these ratios with increasing depths reflects changes in the spectral shape of GCR particles with greater depths (there being relatively more low-energy particles) and the differences in the excitation functions for the reactions producing these two isotopes.

Fig. 4. A comparison of the predicted and observed cosmic-ray-produced Kr isotopes for all samples in Table 3. R_p is the predicted and R_o is the observed ratio of each isotope relative to ^{83}Kr. The points connected by lines and the two boxes represent the range of values for the two depths used for 67015 and 67075. For ^{80}Kr and ^{82}Kr, the left column includes the $Br(n,\gamma)$ contribution; the right column does not.

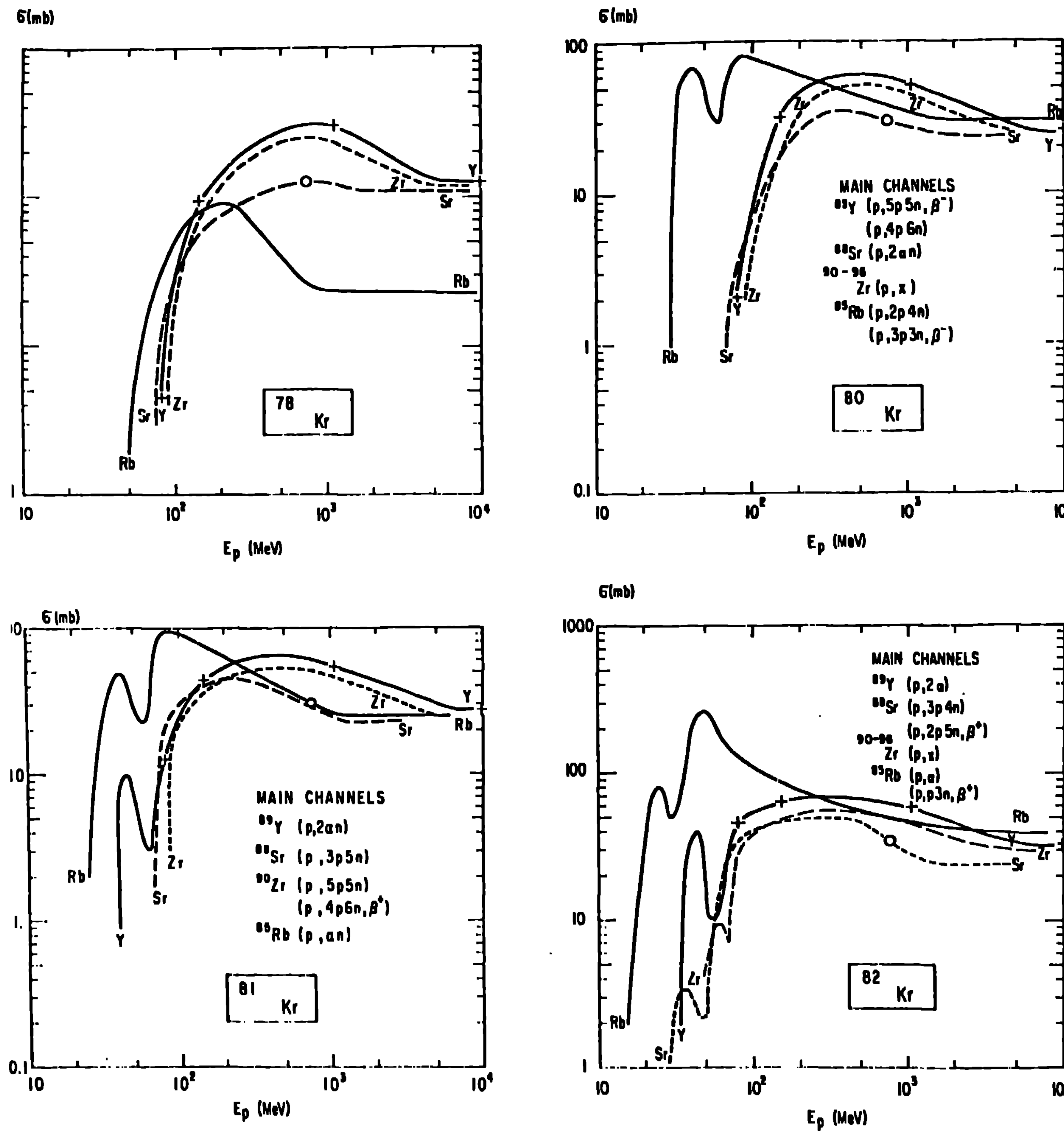

σ(mb)
78 Kr
Rb
Sr
Y
Zr
10
10²
10³
10⁴
Eₚ (MeV)
σ(mb)
100
10
1
0.1
MAIN CHANNELS
⁸⁹Y (p,5p5n,β⁻)
(p,4p6n)
⁸⁸Sr (p,2αn)
90-96
Zr (p,x)
⁸⁵Rb (p,2p4n)
(p,3p3n,β⁻)
80 Kr
Eₚ (MeV)
σ(mb)
MAIN CHANNELS
⁸⁹Y (p,2αn)
⁸⁸Sr (p,3p5n)
⁹⁰Zr (p,5p5n)
(p,4p6n,β⁺)
⁸⁶Rb (p,αn)
81 Kr
Eₚ (MeV)
σ(mb)
1000
MAIN CHANNELS
⁸⁹Y (p,2α)
⁸⁸Sr (p,3p4n)
(p,2p5n,β⁺)
90-96
Zr (p,x)
⁸⁵Rb (p,α)
(p,p3n,β⁺)
82 Kr
Eₚ (MeV)

Fig. 1

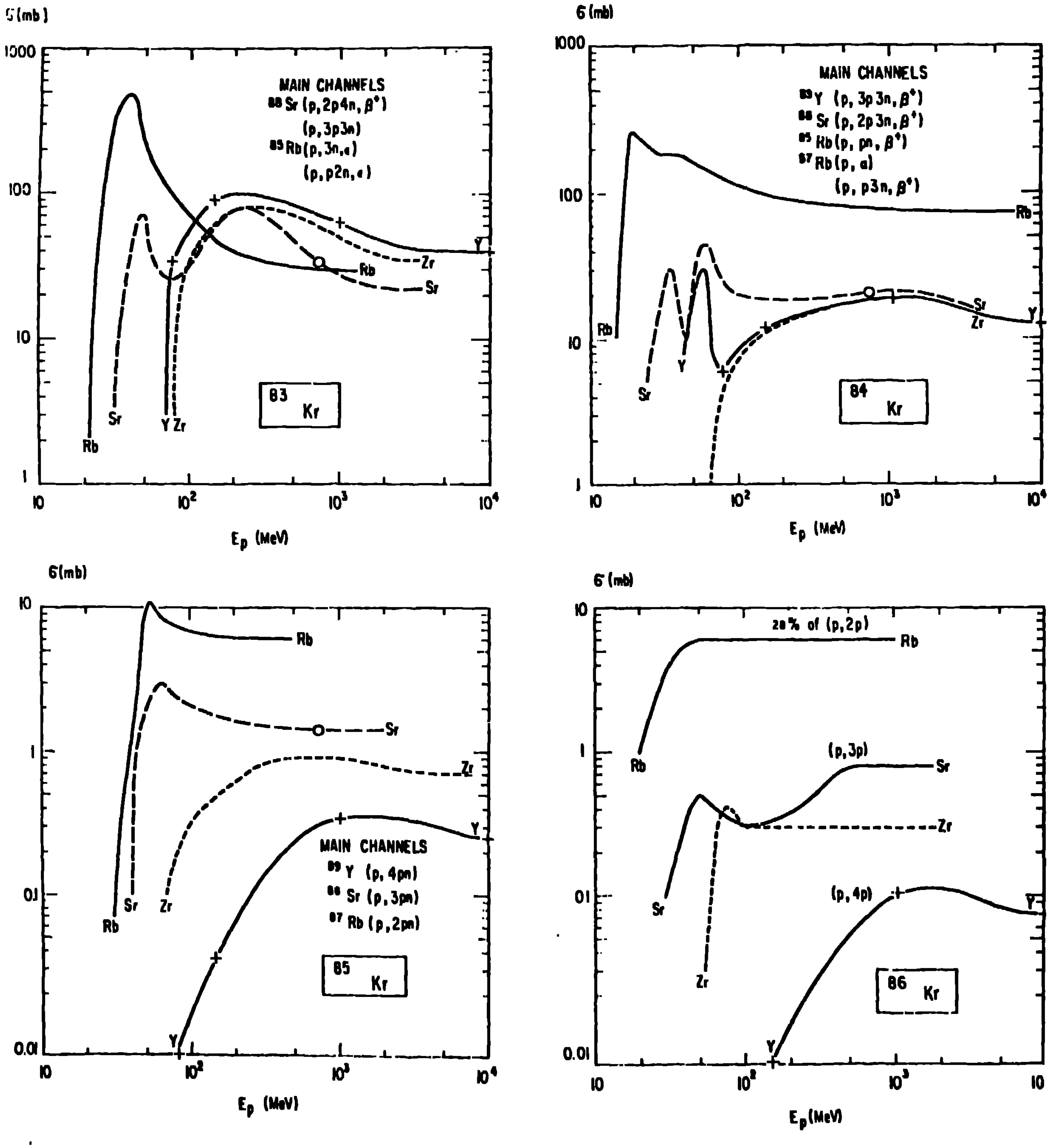
σ (mb)
MAIN CHANNELS
^{88}Sr (p,2p4n,β$^+$)
(p,3p3n)
^{85}Rb(p,3n,ε)
(p,p2n,ε)
83 Kr
Rb
Sr
Y
Zr
E$_p$ (MeV)
σ (mb)
MAIN CHANNELS
^{89}Y (p,3p3n,β$^+$)
^{88}Sr (p,2p3n,β$^+$)
^{85}Rb (p,pn,β$^+$)
^{87}Rb (p,α)
(p,p3n,β$^+$)
84 Kr
E$_p$ (MeV)
σ (mb)
MAIN CHANNELS
^{89}Y (p,4pn)
^{88}Sr (p,3pn)
^{87}Rb (p,2pn)
85 Kr
E$_p$ (MeV)
σ (mb)
28% of (p,2p)
(p,3p)
(p,4p)
86 Kr
E$_p$(MeV)

Fig. 2

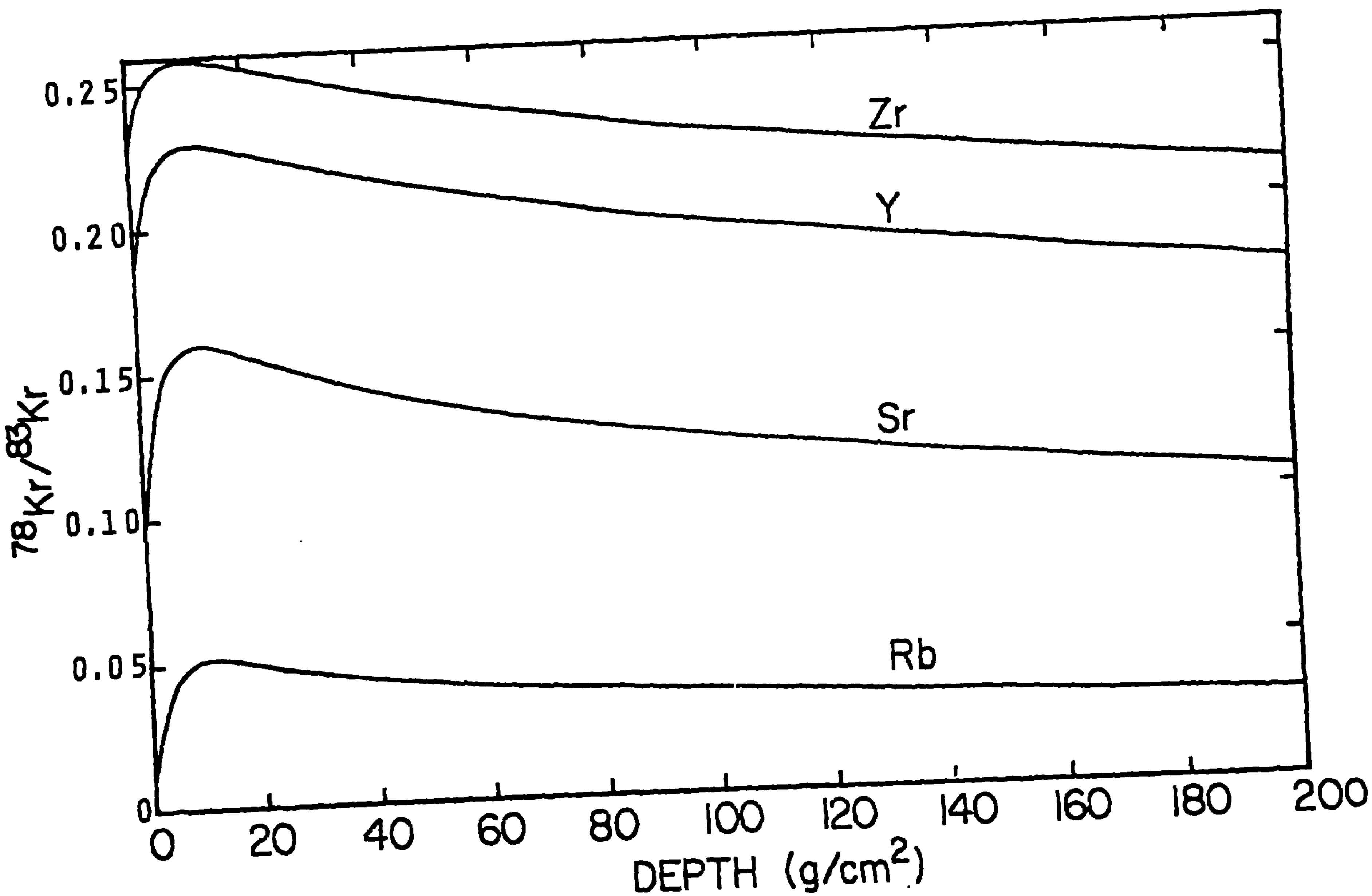
0.25
0.20
0.15
0.10
0.05
0
$^{78}Kr/^{83}Kr$
Zr
Y
Sr
Rb
0
20
40
60
80
100
120
140
160
180
200
DEPTH (g/cm^2)

Fig. 3

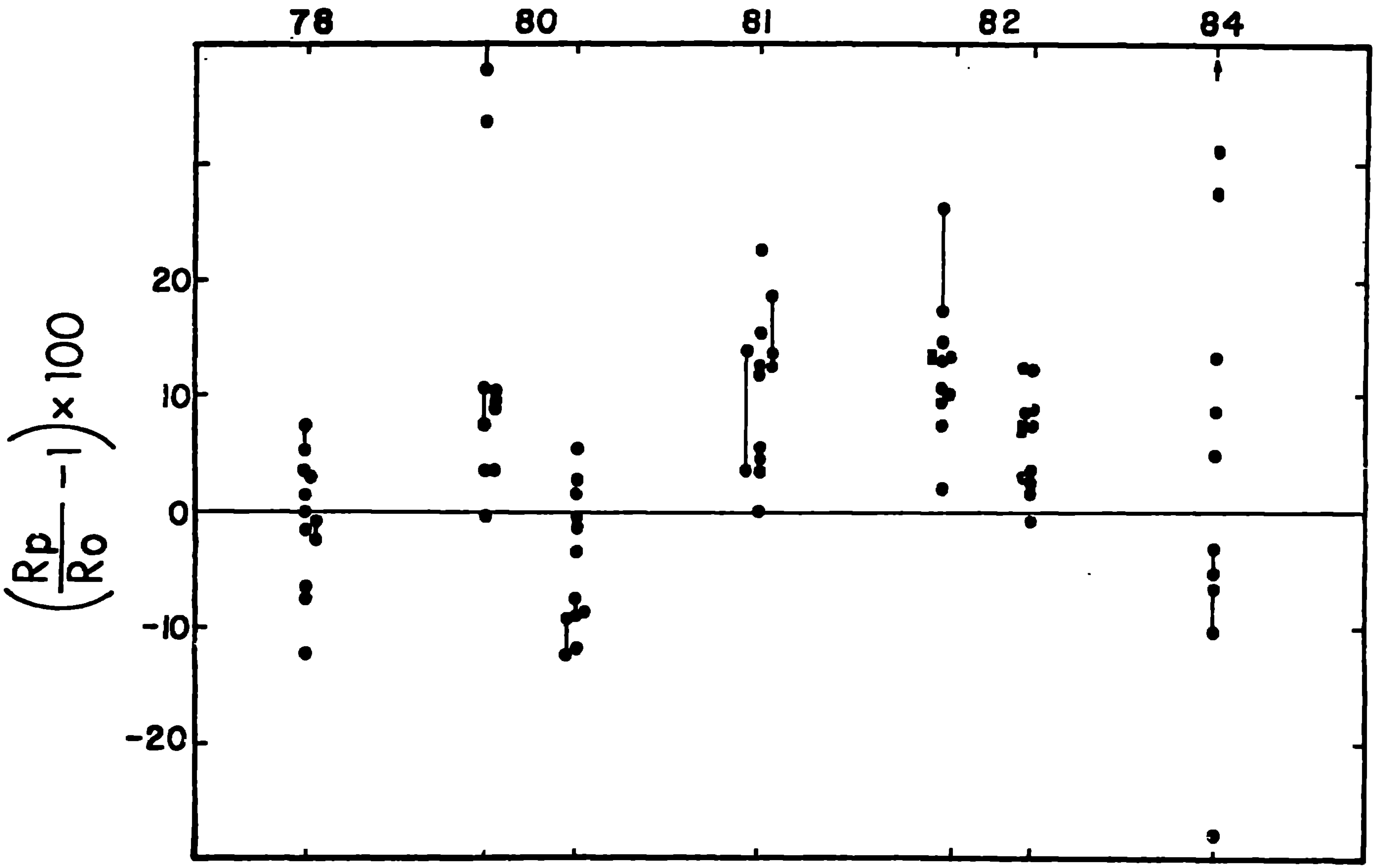

Fig. 4